STUDIES ON THE FORMATION OF NANOPARTICLES OF HYDROXYAPATITE IN AQUEOUS SOLUTIONS

A DISSERTATION SUBMITTED

BY

PURNIMA. N

IN PARTIAL FULFILMENT OF THE REQUIREMENTS

FOR THE DEGREE OF

MASTER OF PHILOSOPHY

SREE CHITRA TIRUNAL INSTITUTE FOR MEDICAL SCIENCES AND TECHNOLOGY

TRIVANDRUM – 695 011

DECLARATION

I, **Purnima N**, hereby declare that I had personally carried out the work depicted in the dissertation entitled "STUDIES ON THE FORMATION OF NANOPARTICLES OF HYDROXYAPATITE IN AQUEOUS SOLUTIONS" under the direct supervision of **Dr. Manoj Komath,** Scientist-E, Bioceramics Lab, Biomedical Technology Wing, Sree Chitra Tirunal Institute for Medical Sciences and Technology, Thiruvananthapuram, Kerala, India. External help sought are acknowledged.

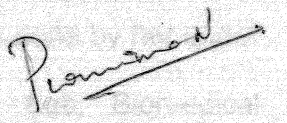

Purnima N.

DECLARATION

I, **Purnima N**, hereby declare that I had personally carried out the work depicted in the dissertation entitled "STUDIES ON THE FORMATION OF NANOPARTICLES OF HYDROXYAPATITE IN AQUEOUS SOLUTIONS" under the direct supervision of **Dr. Manoj Komath,** Scientist-E, Bioceramics Lab, Biomedical Technology Wing, Sree Chitra Tirunal Institute for Medical Sciences and Technology, Thiruvananthapuram, Kerala, India. External help sought are acknowledged.

Purnima N.

SREE CHITRA TIRUNAL INSTITUTE FOR MEDICAL SCIENCES & TECHNOLOGY
TRIVANDRUM – 695011, INDIA

(An Institute of National Importance under Govt. of India with the status of University by an Act of Parliament in 1980)

CERTIFICATE

This is to certify that the dissertation entitled '**STUDIES ON THE FORMATION OF NANOPARTICLES OF HYDROXYAPATITE IN AQUEOUS SOLUTIONS**' submitted by **Purnima. N** is in partial fulfilment for the Degree of **Master of Philosophy in Biomedical Technology** to be awarded by this Institute. The entire work was done by her under my supervision and guidance at Bioceramics Lab, Biomedical Technology Wing, Sree Chitra Tirunal Institute for Medical Sciences and Technology (SCTIMST), Thiruvananthapuram-695012.

Thiruvananthapuram

Date : 10. 08. 2010

Dr. Manoj Komath

The Dissertation

Entitled

STUDIES ON THE FORMATION OF NANOPARTICLES OF HYDROXYAPATITE IN AQUEOUS SOLUTIONS

Submitted by

Purnima N.

for

Master of Philosophy

of

SREE CHITRA TIRUNAL INSTITUTE FOR MEDICAL SCIENCES AND TECHNOLOGY
TRIVANDRUM – 695 011

Evaluated and approved

by

Supervisor
(Name and designation)
Dr. Manoj Komath
Scientist-E
BMT Wing, SCTIMST

Examiner
(Name and designation)
Dr. S. Anantharamaiah
Scientist, NIIST/TVM

Acknowledgement

I sincerely thank Dr. P. R. Harikrishna Varma, Scientist In Charge, Bioceramics Laboratory, Sree Chitra Tirunal Institute for Medical Sciences and Technology, Thiruvananthapuram, for offering support and extending the necessary facilities to carry out this work.

I express my gratitude to my supervising guide Dr. Manoj Komath, Scientist-E, Bioceramics Laboratory, Sree Chitra Tirunal Institute for Medical Sciences and Technology, Thiruvananthapuram, for his guidance and support throughout the course of this project work.

I am grateful to Dr. Lissy Krishnan, SCTIMST, our course coordinator, for the support and encouragement.

I am sincerely thankful to Dr. P. Padmaja, Dr. Sailaja, Mr. Suresh Babu, Mr. S. Vijayan, and Mr. R. Sreekumar for their valuable guidance, support and encouragement.

I am greatly thankful to Mr. Sreekanth P.J, Mr. Rajesh. P, Mr. Nishad. K.V, Mr. Sanoj M.A and Mr. Jijin R.V for extending kind co-operation and support for the successful completion of the work. I would like to thank Mr. Willi Paul, Miss. Nimmi and Miss. Susan for the technical support for the measurements done in their labs.

I am greatly indebted to my parents, other family members and friends for their kind co-operation, intense support, motivation and encouragement throughout the course of my work.

Above all, I thank the Almighty for bestowing on me, a great opportunity and the privilege to gain valuable experience in the field of experimental and analytical study of science by working in this project at Sree Chitra Tirunal Institute for Medical Sciences and Technology, Thiruvananthapuram.

Purnima. N

CONTENTS

List of Figures

List of Tables

List of abbreviations

Abbreviation	Expansion
HAp	Hydroxyapatite
XRD	X-ray Diffraction
DLS	Dynamic Light Scattering
TEM	Transmission Electron Microscopy
SEM	Scanning Electron Microscopy
EDS	Energy Dispersive X-ray Spectroscopy
ICP	Inductively Coupled Plasma Technique
AES	Optical Emission Spectroscopy
IAP	Ionic Activity Product
SBF	Simulated Body Fluid

Synopsis

Hydroxyapatite [HAp] is an important material in medicine, being the basic bone mineral. HAp ceramics are widely used in orthopaedics in various forms for bone grafting since it is biocompatible and osteoconductive. Active research is ongoing to make HAp ceramics from nano-sized particles so as to achieve improved mechanical properties and nano-level porosity. Design of nanoceramics of HAp needs deeper understanding of the formation of nano-particles from aqueous solutions. This work is an attempt to fill the knowledge gap in the nucleation and growth kinetics of hydroxyapatite from aqueous solutions, with a view to study the effects of parameters like the reaction temperature, on the particle size formed.

Chapter 1 gives an introduction to HAp as a biomaterial with descriptions on its composition, structure and properties. The conventional methods adopted for synthesis of HAp from solutions are described. The gaps identified based on the literature review on synthesis, processing and applications of HAp are explained, followed by the research objectives.

Chapter 2 describes the materials and methods related to the work carried out to explore the research objectives. Temperature-controlled wet precipitation synthesis of HAp (from 5℃ to 80℃) was done using $Ca(NO_3)_2.4H_2O$ and $NH_4H_2PO_4$ solutions maintained at basic pH. X-Ray Diffraction (XRD) and Fourier Transform Infrared Spectroscopy (FTIR) were used to confirm the phase of the precipitate. The Ca/P ratios in the precipitates were determined by Atomic Emission Spectroscopy (AES-ICP). Particle size measurements are done using the Debye-Scherrer method in XRD, Dynamic Light Scattering (DLS) and Transmission Electron Microscopy (TEM). The particles obtained at various temperatures were made into ceramic pellets through conventional ceramic processing, by sintering at 1150℃. The densities are measured using Archimedes apparatus and the Vicker's microhardness through microindentation. The microstructural aspects are investigated by Environmental Scanning Electron Microscopy (ESEM). The sample preparation methods and analysis modes are described for all the studies.

Chapter 3 includes the results of the studies and related discussion of various aspects. XRD and FTIR showed the precipitated phase to be pure hydroxyapatite. AES-ICP analysis gave the Ca/P ratios nearly equal to that of the theoretical composition of HAp. A variation in particle size in the nano-range was evident form the XRD spectral peak-broadening. The particle size analysis, done through three different techniques showed that the size of the precipitated HAp particles was directly related to the synthesis temperature. The sizes varied from ~ 40 nm to ~120 nm in the range of synthesis temperatures from 5℃ to 80℃. The TEM images revea l the particles' shape and their existence as chains/aggregates.

The ceramic pellets made out of these particles (synthesized at various temperatures) show comparable densities, but varying Vicker's microhardness (H_V). Corresponding to the synthesis temperatures from 5℃ to 80℃, the H_V values increased by approximately three times. The highest recorded value, i.e., for the 80℃ sample, is 581.67 HV, which is t he highest reported for HAp ceramic.

The microstructure analysis of the sintered samples by ESEM shows larger grain size for the lower temperature-synthesized HAp ceramic and smaller grain size for the higher temperature-synthesized HAp ceramic. This explains the microhardness behavior.

Chapter 4 gives the summary and conclusion based on the results of various studies. The study shows that, in aqueous precipitation, hydroxyapatite starts forming as nanoparticles. It is possible to synthesize a desired set of nano-sized HAp from aqueous solution by optimizing the reaction parameters. Highly dense and hard ceramic could be produced with nano-sized HAp by carefully adjusting the sintering temperature. Such nano-structured HAp ceramics are highly useful in certain orthopaedic applications like vertebro-laminoplasty.

Studies on nucleation and crystal growth of HAp from aqueous solutions give valuable information for useful applications. Many such correlations are to be explored further. A better understanding of sintering may help in developing clinically useful hydroxyapatite ceramics.

Chapter 1

INTRODUCTION

1.1 Background

1.1.1 The apatites

The term apatite describes a family of compounds having similar structure in spite of a wide range of composition. These crystalline minerals have the common formula $X_{10}(YO_4)_6(Z)_2$ where,

X -- Ca, Sr, Ba, Cd, Pb, Mg, Na, K, H

Y -- P, V, As, S, Si, Ge, B, CO_3

Z -- OH, CO_3, O, BO_2, halogens.

Depending upon the X, Y and Z ratios, different types of apatite having a variety of properties could be made. Some important examples are,

Fluorapatite	----	$Ca_{10}(PO_4)_6F_2$
Chlorapatite	----	$Ca_{10}(PO_4)_6Cl_2$
Hydroxylapatite	----	$Ca_{10}(PO_4)_6(OH)_2$
Podolite	----	$Ca_{10}(PO_4)_6(CO_3)$
Dahlite	----	$Ca_{10}(PO_4,CO_3)_6(OH)_2$
Francolite	----	$Ca_{10}(PO_4,CO_3)_6(F,OH)_2$

Most of these apatites are present in the igneous rocks and are greatly phosphorous-bearing apatites. Biological apatite forms the mineral phase of calcified tissue (bone, enamel and dentin). Hydroxylapatite (or hydroxyapatite) with the chemical formula $[Ca_{10}(PO_4)_6(OH)_2]$, is therefore, of special interest in biology and medicine.

1.1.2 Hydroxyapatite

Natural bone mainly consists of substituted forms of hydroxyl apatite (hydroxyapatite). It differs from pure hydroxyapatite (‘***HAp***’) in stoichiometry, composition, crystallinity and also in other physical and mechanical properties. Biological apatites are usually calcium-deficient and carbonate-substituted.

Hydroxyapatite [Ca_{10} $(PO_4)_6$ $(OH)_2$], due to its structural similarity with the bone mineral and biocompatibility, is found to be an ideal bone substitute material.

1.1.3 Crystal structure of hydroxyapatite

The crystal structure of natural apatite was determined by Naray-Szabo and Mehmel independently in 1930. The details about hydroxyapatite crystals could be summarized as follows:

Molecular weight → 1004.8
Crystal system → Hexagonal
Space b group → $P6_3/m$
Lattice constants → a = 9.423Å, c = 6.875 Å
Density → 3.16 g/cm^3
The Ca/P ratio → 1.67.

Hydroxyapatite (HAp) is the most stable phase among the various calcium phosphates and is stable in body fluids; dry or moist air up to 1200°C.

There are two crystallographically independent Ca atoms in the unit cell of the HAp crystal. Each Ca-II atom is surrounded by six atoms belonging to PO_4 groups and an OH group, whereas the Ca-I atom is nearly octahedrally surrounded by six O atoms. The Ca-II atoms form a triangle normal to the C-axis. The Ca-II triangles stack along the C-axis, rotating mutually 60° from each other. The OH group is shifted above or below the centre of the Ca-II triangle. The P atom and the four O atoms surrounding it together form a tetrahedron. The PO_4 tetrahedron is almost regular with only a slight distortion.

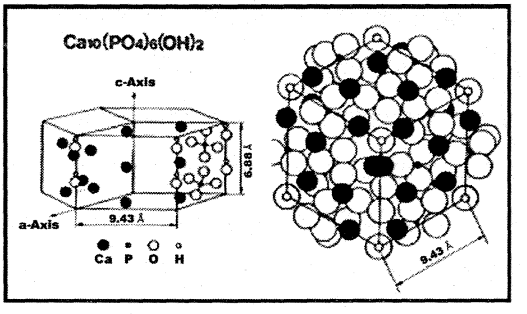

Fig.1.1 ***Crystal structure of Hydroxyapatite projected along the C and A- axes***

Substitutions in the apatite structure for Ca, PO_4 or OH groups change properties such as lattice parameters, morphology and solubility without changing the hexagonal symmetry. Chloride [Cl^-] substitution changes the hexagonal symmetry and shows monoclinic symmetry. Substitution of F for OH results in contraction of the A-axis dimension without changing the C-axis resulting in an increase in crystallinity and greater stability of the structure. Hydroxyapatite is almost isostructural with fluorapatite.

1.1.4 Composition of hydroxyapatite

Pure HAp has a theoretical composition of 39.68 wt% Ca, 18.45 wt% P, Ca/P wt ratio 2.151 and Ca/P molar ratio of 1.667. The variations in Ca/P ratio reflect the purity; i.e. whether it consists of only the apatite phase or is mixed with other calcium phosphate phases. If the Ca/P ratio is 1.67, the HAp phase could be considered pure. A lesser Ca/P ratio results in β-tricalcium phosphate [β-TCP], and a higher ratio gives tetracalcium phosphate [TTCP], $Ca_4P_2O_9$ or $Ca_4(PO_4)_2O$.

The purity, composition and particle size of the apatite prepared, will depend on the synthesis parameters, sintering temperature and other conditions. Also the starting materials (calcium and phosphate based reactants in the synthesis) have role in the quality of the final product. In bulk production, the choice of starting materials decides the cost of the product.

1.1.5 Other calcium phosphates

Calcium phosphates occur in a series of phases with varying calcium and phosphate ion combinations. These compounds exist in both amorphous and crystalline forms. The Ca/P ratio is considered ideal to define them. Table 1.1 presents the important calcium phosphate compounds classified based on their Ca/P ratios. The Ca/P ratio varies from 2 (Hilgenstockite) to 0.5 (monocalcium phosphate monohydrate). Generally, calcium phosphates with higher Ca/P ratios (>1.5) are precipitated in an alkaline medium while those with lesser Ca/P ratios need acidic conditions.

Table-1.1 Calcium Phosphate compounds			
Ca/P	***Formula***	***Name***	***Abbreviation***
2.0	$Ca_4O(PO_4)_2$	Tetra-calcium Phosphate (Hilgenstockite)	TTCP
1.67	$Ca_{10}(PO_4)_6(OH)_2$ $Ca_{10-x}H_{2x}(PO_4)_6(0H)_2$	Hydroxyapatite Amorphous Calcium Phosphate	HAp ACP
1.50	$Ca_3(PO_4)_2$	Tri-calcium Phosphate	TCP
1.33	$Ca_8H_2(PO_4)$	Octacalcium Phosphate	OCP
1.0	Ca_2HPO_4	Dicalcium Phosphate (Monetite)	DCP
1.0	$Ca_2P_2O_7$	Calcium Pyrophosphate	CPP
1.0	$Ca_2P_2O_7.2H_2O$	Calcium Pyrophosphate Dihydrate	PPD
0.7	$Ca_7(P5O_{16})_2$	Hepta-calcium Phosphate (Tromelite)	HCP
0.67	$Ca_4H_2P_6O_{20}$	Tetra-calcium dihydrogen phosphate	TDHP
0.5	$CaH_2(PO_4)2H_2O$	Mono-Calcium Phosphate Monohydrate	MCPM
0.5	$Ca(PO_3)_2$	Calcium Meta Phosphate	CMP

1.2 Synthesis and characterization of hydroxyapatite

1.2.1 Preparation of hydroxyapatite

Various techniques have been used for the preparation of HAp. The desired phase could be made from appropriate reactants in the Ca/P ratio corresponding to HAp, through wet precipitation, high-temperature processing, high-pressure processing and chemical reactions. There are four important methods for the preparation of HAp.

(i) Wet method
(ii) Dry method
(iii) Hydrothermal method
(iv) Alkoxide method

These are described in the following sections.

(i) Wet method

Wet method is used for the bulk production of small crystalline or non-crystalline HAp powder. The method is based on the following equation.

$$10\ (CaNO_3)_2 + 6\ (NH_4)H_2PO_4 + 14\ NH_4OH \rightarrow Ca_{10}(PO_4)_6(OH)_2 + 20\ NH_4NO_3 + 12\ H_2O$$

Here the reagents are taken as ammoniated solutions (pH ≈ 10).

(ii) Dry method

This is done at high temperatures using reagents in the solid state, i.e. in powder form. This method is well suited for preparing highly crystalline HAp powder. For example, with $CaHPO_4.2H_2O$ and $CaCO_3$ as the starting materials, the following reaction will occur:

$$6\ CaHPO_4.\ 2H_2O + 4\ CaCO_3 \rightarrow Ca_{10}\ (PO_4)_6\ (OH)_2 + 14\ H_2O$$

HAp prepared by this method is very fine and highly crystalline. However, impurity phase is the major problem with this method.

(iii) Hydrothermal method

Hydrothermal synthesis can be defined as a method of synthesis of single crystals which depends on the solubility of minerals in hot water under high pressure. Crystal growth is performed in an apparatus consisting of a steel pressure vessel called autoclave, in which a nutrient is supplied along with water. A gradient of temperature is maintained at the opposite ends of the growth chamber so that hotter end dissolves the nutrient and cooler end causes the seeds to take additional growth.

This method is preferred for obtaining large, perfect single crystals of hydroxyapatite. Normally, HAp prepared by wet method in the atmosphere consists of very small crystals with lattice defects. This problem is eliminated with hydrothermal method. Hydrothermal synthesis includes various techniques of crystallizing substances from high-temperature aqueous solutions at high vapour pressures.

(iv) Alkoxide method

This is a recently introduced method for preparing thin hydroxyapatite films. A reaction involving calcium nitrate tetra-hydrate and tri-methyl phosphate as starting materials, with ethanol or formamide is represented below. After the solvent is vaporized, the mixture of the starting materials is heated at 50℃ -1000℃ to produce well-crystallized HAp.

$$Ca(NO_3)_2.4H_2O + (CH_3O)_3PO \rightarrow Ca_{10}(PO_4)_6(OH)_2$$

1.2.2 Characterization of hydroxyapatite

(i) Phase identification

The crystal structure and phase composition of HAp can be determined through the X-ray diffraction technique (XRD). The X-ray diffractometer directs a collimated X-ray beam onto powdered sample and records a plot of the intensity of the diffracted X-rays from various atomic planes against the angle of incidence. The characteristic diffraction pattern of HAp can be verified by comparing with the JCPDS/ICDD standards.

(ii) Functional groups identification

Fourier Transform Infrared Spectroscopy (FTIR) could be used to identify the various functional groups in HAp. The equipment identifies the infrared absorptions due to vibrational energy transitions of the molecule in the region 400 cm^{-1} to 4000 cm^{-1}. The characteristic absorbance/transmittance peaks corresponding to the functional groups constituting the molecule could be determined and the phase could be confirmed.

(iii) Surface microstructure

Scanning Electron Microscopy (SEM) is highly useful in analyzing the microstructural features of HAp ceramics. Dried and polished specimens are kept under the scanning beam after coating the surface with gold. By using backscattered and secondary electron detectors, detailed information like the overall morphology, grain size, grain distribution, porosity etc could be collected.

(iv) Elemental composition and Ca/P ratio

The elemental composition in HAp could be determined and quantified using atomic emission spectroscopy (AES-ICP). A known quantity of the sample is fully dissolved in an aqueous medium (acid) and atomized into an argon flame created with RF plasma. The emission spectra of the elements in the sample are recorded and from the characteristic peaks of the elements, quantification could be done to parts-per-million level. Standard solutions of Ca and P could be used to make the calibration plot of absorbance versus concentration, from which quantification could be done. The Ca/P ratio can be determined from the Ca and P concentrations obtained from the plot.

Another method for elemental detection is the Energy Dispersive X-ray Spectroscopy (EDS), which comes as an attachment to SEM instrument. The presence of Ca and P can be ensured by EDS.

(v) Pore volume and distribution

Mercury intrusion porosimetry and Micro CT give information on the pore volume and distribution of the material.

(vi) Compressive strength and microhardness

Mechanical properties of HAp ceramic like compressive strength and flexural strength can be determined using Universal Testing Machine (UTM). Known values of load are applied on appropriately made specimens and the breakdown events are recorded.

Vickers microhardness of the ceramic can be determined in micro-indentation hardness tester. Impressions are made on the surface using a pyramidal diamond indenter under a known load and the hardness value is calculated from the dimensions of the indentation mark.

(vii) Particle size analysis

Wet synthesis of hydroxyapatite usually generates nano-level crystals at the early stages of the process. These could be visualised using Transmission Electron Microscopy (TEM). The particle size distribution can be analyzed with Dynamic Light Scattering (DLS) technique.

1.2.3 Medical applications of HAp

The major application of hydroxyapatite material is as synthetic bone graft. Being the bone mineral, HAp has excellent biocompatibility and the capacity to integrate with host bone. Porous ceramic forms of HAp have been proven to be successful as substitutes to natural bone graft. Currently hydroxyapatite ceramics in various shapes and forms are used for numerous bone grafting procedures in orthopaedics and dentistry. The granule form is used as bone filler. Shapes like blocks, rods and discs with different porosities are being used. As hydroxyapatite is soft-tissue compatible, it is used in percutaneous devices. Also, porous HAp is used for drug delivery applications. Several HAp based products are in the market for clinical applications.

1.3 Review of literature

Development of HAp products for biomedical applications demands stringent and consistent quality. Ensuring the quality of the final product starts from the synthesis of particles of controlled size and phase. These factors decide the microstructure, which in turn determines the mechanical and biological performance of the product. Therefore, detailed studies of various aspects right from precipitation parameters and reaction kinetics to ceramic processing are needed to make a reliable product.

Out of the various methods of hydroxyapatite synthesis, the precipitation method has been found to be of great advantage. Because of homogeneous chemical mixing, precursors produced by this method have short component diffusion distances. Better control over reaction parameters such as temperature, pH, concentration of reagents etc. is achievable during synthesis. Also, the wet method has commercial potential for bulk production. Therefore it is decided to study the precipitation characteristics of hydroxyapatite in aqueous solutions. A literature review in this regard is presented in the following section.

1.3.1 Studies on the formation of hydroxyapatite

Hydroxyapatite can be synthesized through a number of diverse processes. Wet chemical synthesis is one among them [1-3]. In wet-chemical route, HAp is precipitated from either an acid-base reaction or a reaction between various salts. Other methods include the sol-gel technique [4], solid-state reactions at elevated temperatures [5] and biosynthesis routes [6]. Among the different synthesis methods, the wet precipitation method of synthesizing HAp is the most popular, as it offers better control over the particle size and morphology of the precipitates, which can be achieved by varying the concentration of calcium and phosphate ions as well as the pH of the reaction medium when compared to other methods. The functionality of HAp in biological environments such as bioactivity, physical and chemical stability and mechanical properties depends on the particle size, morphology and stoichiometry of the synthesized HAp powders [7-9].

It is well-documented that the physical, chemical, and biological properties of the synthesized HAp, depends on its morphology, crystallite size, purity, stoichiometry, and structure [10-12]. Therefore, control of morphology is of great importance as the final size and shape of the HAp crystallites influence the cell compatibility, osseointegration, and resorption of orthopaedic or otherwise intended devices. The morphology of the HAp precipitates changes from needle-like to nearly spherical, or, the aspect ratio (length-to-diameter ratio) decreases as the reaction temperature is increased when it is synthesized using $Ca(OH)_2$ and H_3PO_4 [13,14]. In contrast, the morphology of HAp particles changes from elongated spherical to columnar (rod-like) or the aspect ratio increases with increasing temperature when soluble calcium salts such as $Ca(NO_3)_2$ and $CaCl_2$ and phosphate salts in basic medium are used [14].

The resultant morphology of a precipitate may be described in terms of its precipitation kinetics [15]. A higher precipitation rate yields particles with higher aspect ratio, and as the precipitation rate is decreased the aspect ratio decreases. The precipitation rate depends on the driving force for precipitation, which in turn depends on the reaction temperature, T, ionic activity product (IAP) and the solubility product, $k$sp, with respect to the precipitating

compound. The driving force for the precipitation of HAp at a given temperature is the difference in Gibbs free energy, ΔG_{HAp}, between the supersaturated and equilibrium solutions of HAp and is mathematically expressed by equation (1) where IAP is the ionic activity product expressed in equation (2), (in which the bracketed species represent the concentrations of ions and the ç values are the activity coefficients of ions), k_{sp} is the solubility product of HAp, 'v' is the number of ions (5 + 3 + 1) 9 for HAp), R is the universal gas constant (8.314 J/mol. K), and T is the absolute temperature.

$$\Delta G_{HA} = -\frac{RT}{\upsilon}\ln\frac{IAP}{k_{sp}} \qquad (1)$$

$$IAP = [Ca^{2+}]^5[PO_4^{3-}]^3[OH^-]\gamma_{Ca^{2+}}{}^5\gamma_{PO_4^{3-}}{}^3\gamma_{OH^-} \qquad (2)$$

Heterogeneous nucleation occurs only on the surfaces of foreign bodies when there are special objects inside a phase that can cause nucleation because of lower free energy. Therefore, it is important to maintain the solution stable. In other words, no particle is present in the solution. In such a case, preferential nucleation of HAp always occurs on the negative surfaces.

Homogeneous nucleation occurs when there are no special objects inside a phase that can cause nucleation, or in other words, it occurs only in solution. Homogeneous nucleation will be initiated on increasing the degree of supersaturation[16]. Actually, during the initial stage of homogeneous nucleation, the solute molecules (or atoms) combine to produce clusters, or "embryos". When the supersaturation degree is less than one (S<1.0), G(r) is always positive and cluster formation does not occur. When the supersaturation degree exceeds one (S > 1:0), G(r) has a positive maximum at the critical size, r* with a maximum Gibbs free energy, G_{max} = G(r*).

This is the classical energy barrier for nucleation. The free energy of clusters larger than the critical size will decrease by further growth, producing 'stable nuclei' that grow to form macroscopic particles. Below the critical size, the free energy of clusters decreases by dissolution. Ito et al. [17] confirmed the presence of calcium phosphate clusters from 0.7 nm to 1.0 nm in size in SBF by using an intensity-enhanced dynamic light-scattering technique. Therefore,

the formation of calcium phosphate particles can be easily induced by increasing ionic concentrations or pH values in the solutions in a short time even before the heterogeneous nucleation occurs.

Theoretically, homogeneous nuclei are formed by aggregates of several clusters of critical size. The homogeneous nuclei are expected to have three special characteristics: very small size (several nm), charged surface, and progressive growth of high chemical activity. The critical radius *r* of the cluster is given by

$$r^* = \frac{2\sigma_{SL}v^2}{kT\ln S}$$

Where σ_{SL} is the solid–liquid interfacial energy (J/m^2), 'v' the molecular volume (m^3/mol), 'k' the Boltzmann constant, 'S' the supersaturation degree, and 'T' the absolute temperature (K). The charged conditions of the particle depend on some factors, such as the specific adsorbed layer, the ionic strength of the solution, pH, particle size and shape. Moreover, the charged surfaces and non-stoichiometric states of homogeneous nuclei give rise to high chemical reactivity, which becomes the driving force for their further growth by consumption of ions from solution. Therefore, we can produce chemically reactive particles with appropriate size and surface charge, by controlling homogeneous nucleation in a supersaturated solution [18].

Significant differences in the chemical composition, morphology, and amorphous character of the HAp nanoparticles could be made effective through the reaction between $Ca(NO_3)_2$ (aq) and $(NH_4)_2HPO_4$ (aq) by changing the time of reaction, temperature and pH of the reaction mixture. Prakash et al recently reported that HAp synthesized through acid-base reaction at a range of temperatures show that the morphology of the particles changed from needle-shaped at 40℃ to spheroidal at 100℃ [19].They found that even though the morphology changed, the predominant phase at all the temperatures was HAp (ensured with X-ray diffraction patterns). According to them, the driving force for the morphological changes during HAp precipitation is mainly the supersaturation level of Ca^{2+} and PO_4^{3-} ions with respect to HAp. The analysis

also indicated that the super saturation level of the reactant solutions, especially the concentration of Ca^{2+} ions, played a predominant role on the precipitate morphology for this classical acid-base reaction.

As it is well-known that HAp is osteoconductive, synthetic HAp has been widely used in hard tissue repair applications, such as implant coatings and bone substitutes. Nanocrystalline HAp exhibits better bioactivity and also biocompatibility with enhanced mechanical properties compared to the microcrystalline counterpart. Methods that have been used for preparing nano HAp include chemical precipitation in some cases followed by spray drying or hydrothermal treatment sol-gel approach, microemulsion techniques, precipitation from complex solutions followed by microwave heating, wet chemical methods incorporating a freeze drying step, mechanochemical synthesis and electrodeposition [20].

Depending upon the synthesis technique, materials with various morphology, stoichiometry, and level of crystallinity can be obtained. It is possible to improve the properties of HAp ceramics by controlling important parameters of powder precursors such as particle size, particle distribution and agglomeration [21]. Nanocrystalline HAp powders have greater surface area and are expected to have better bioactivity than coarser crystals [22,23]. Osteoconductivity, solubility, sinterability and mechanical reliability of HAp can be promoted by controlling its particle size and structural morphology in the order of nanoscale [21,24].

In a recent study, it has been reported that the solvent also has a role in determining the morphology of HAp powders [26]. HAp powder was prepared by a high temperature flame spray pyrolysis process from various types of spray solution and found that the volume ratio of ethyl alcohol in the mixed solvent plays a key role in obtaining nanosized HAp powders with spherical shape. The morphologies of the HAp powders were affected by the volume ratio of ethyl alcohol and distilled water in the mixed solvent. The number of nano-sized HAp powder particles increased with an increase in the volume ratio of ethyl alcohol to distilled water in the mixed solvent. The mean size of the HAp powders measured from the TEM image was 37 nm.

1.3.2 Gaps identified

Studies on the nucleation and growth kinetics of the precipitation reaction of aqueous solutions are required for the optimization of conditions for formulation of well-suited methodologies for obtaining a product with desirable properties. Modification of controllable parameters like concentration (Ca/P ratio), temperature and pH of synthesis, sintering temperature etc. enables the formation of fine, controlled morphology powders which could be processed into the final form. Characterization of individual nanoparticles in situ has been a great challenge in the case of nano HAp due to the difficulty in generalization of dispersion methods since particles have a high tendency of aggregation in solution immediately after the formation of the stable HAp phase. The size and shape of the first nucleus formed in solution at the super-saturation concentration and the time of the first nucleation have been studied less. However, at the physiological pH (i.e., 7.4) and higher, HAp [$Ca_{10}(PO)_6OH_2$] is found to be the most stable calcium phosphate phase.

1.4 The Hypothesis

The nucleation of HAp can be tracked in the $Ca(NO_3)_2.4H_2O$ - $NH_4H_2PO_4$ system at the supersaturation condition. To find the particle size of the calcium phosphate precipitated initially, just when the concentration (S) of the Ca^{2+} and PO_4^{3-} ions in the solution mixture reach the supersaturation value, the following parameters should be finely controlled.

- Supersaturation concentration
- pH of the system
- Ca/P ratio

The Ca and P sources [$Ca(NO_3)_2.4H_2O$ - $NH_4H_2PO_4$ solutions system] could be mixed in various concentrations till the initial precipitate (the first nucleus) is formed. The nucleus formation could be confirmed by DLS method, the minimum limit being 0.6 nm, by analyzing the solution system at definite time intervals, till a particle size is recorded, i.e., at the beginning of nucleation. This concentration at which the initial precipitate (nucleus) is formed should be the supersaturation [S].

The supersaturation value of concentration and the particle size (half of which is the critical radius of the nucleus) could be substituted in the equation for Gibb's free energy of the system with various temperature values of synthesis. The energy should be the minimum for the HAp phase among all the calcium phosphates precipitated.

1.5 Research objectives

1. Study of the nucleation and precipitation conditions of hydroxyapatite [$Ca_{10}(PO_4)_6OH_2$] from aqueous solution supersaturated with calcium and phosphate ions.
2. Study of the influence of temperature of synthesis on the size of the HAp particles precipitated from the supersaturated aqueous solution.
3. Study of the physical properties of ceramics made out of nano-sized HAp particles precipitated from the solutions, through heat treatment (sintering).

Chapter 2

MATERIALS AND METHODS

This work explores the formation of hydroxyapatite from aqueous solution in nano-crystalline form and its potential in making useful ceramic material. As per the aims and objectives, the work is divided into 3 parts:

1. Study of the nucleation and precipitation conditions of hydroxyapatite [$Ca_{10}(PO_4)_6OH_2$] from aqueous solution supersaturated with calcium and phosphate ions.
2. Study of the influence of temperature of synthesis on the size of the HAp particles precipitated from supersaturated aqueous solution.
3. Study of the physical properties of ceramics made out of HAp particles precipitated from the solutions through heat treatment (sintering).

The materials and methods used for each part are described in the following sections.

2.1 Hydroxyapatite nucleation characteristics:

The formation of HAp in an aqueous solution is governed by the theories of nucleation and growth of crystals. It is important to gain sufficient understanding of the nucleation characteristics of HAp in aqueous solution. This could be done by carefully observing the initial stages of formation of calcium phosphate from an aqueous solution supersaturated with calcium and phosphate ions and correlating it with the theory of nucleation.

The system of reagents calcium nitrate tetrahydrate [$Ca(NO_3)_2.4H_2O$] and ammonium dihydrogen orthophosphate [$NH_4H_2PO_4$] is selected for the study. This is a well proven and commercially viable system to precipitate HAp.

2.1.1 Theory of nucleation and growth of Hydroxyapatite:

In the selected system, precipitation of HAp occurs on mixing the corresponding cation [Ca^{2+}] solution [$Ca(NO_3)_2.4H_2O$] with the precipitant medium [$NH_4H_2PO_4$] at the supersaturation condition. The reaction can be represented as follows:

$$10Ca(NO_3)_2.4H_2O + 6NH_4H_2PO_4 + H_2O \rightarrow Ca_{10}(PO_4)_6(OH)_2 + 20NH_4NO_3 + 12H_2O$$

The *driving force for precipitation* is a function of supersaturation [S] given by,

$$\mathbf{S = C / C_e}$$

where C $\rightarrow$ bulk concentration of the species, and

$C_e \rightarrow$ concentration of this species at equilibrium.

The state of *supersaturation* of Ca^{2+} and PO_4^{3-} ions is created in the solution [reaction mixture] through chemical reaction, changes in temperature, pressure, solvent substitution / solvent removal. This condition is relieved and the *free energy* of the system is reduced through spontaneous formation of a particulate solid phase. This happens when the concentrations of the ions in the solution exceeds the solubility limit.

As the minimum energy required for nucleation is reached, the first nucleus is formed. The minimum radius required to begin growth is called the *critical radius*. On reaching this critical size, growth starts and the *Gibb's free energy of the system* decreases, leading to product formation [precipitation] and the system shifts towards the lesser energy side.

For systems with high supersaturation values, nucleation rates increase with increase in supersaturation and consequently, the number of fine particles formed also increases. The most soluble [the least stable] phase is precipitated first, according to the Ostwald rule of stages.

Nucleation of a product from a medium is of two fundamental types:

a. Homogeneous nucleation: Homogeneous nucleation is spontaneous and occurs commonly in solutions.

b. Heterogeneous nucleation: Heterogeneous nucleation involves nucleus formation of the solute on the surface of another entity.

Generally, nucleation occurring in solution reactions for ceramic synthesis is homogeneous which is applicable to the present system also.

In a supersaturated solution, the phenomena of frequent formation and re-dispersion of molecular clusters occur, with energy associated with each cluster given by,

$$E = E_s \textit{ (surface free energy)} + E_v \textit{ (volume free energy)}$$

An energy barrier exists for the product to be formed in a solution. With increase in cluster size, the energy passes through a maximum value [critical free energy for nucleation- E_c] after which stable nuclei are formed, which may be followed by crystal growth.

When a certain minimum size [critical radius - r_c] is attained, the first nucleus is formed. A free energy change [energy reduction] is associated with this phenomenon, which is known as Gibb's free energy change [ΔG]. This is given by the expression,

$$\Delta G = 4\pi r^2 \Delta G_s - (4/3)\, \pi\, r^3 \Delta G_v$$

where $\Delta G_s \rightarrow$ Surface free energy and

$\Delta G_v \rightarrow$ Volume free energy

(assuming spherical nucleus formed)

$G \rightarrow$ Gibb's energy on the formation of a spherical nucleus with radius *r*.

Corresponding to the critical radius r_c, [when [d (ΔG) / dr] = 0],

$$\Delta G_c = 16 \pi G_s^3 / 3 \Delta G_v^3$$

The change in Gibb's free energy for the solutions at different temperatures of synthesis can be calculated using the equation:

$$\Delta G = - RT \ln S$$

$$= - RT \ln (A_p / K_{sp})$$

where G $\rightarrow$ Gibb's free energy (J/Mol)

R $\rightarrow$ Gas constant [8.314 J K^{-1} Mol^{-1}]

T $\rightarrow$ Absolute temperature (K)

n $\rightarrow$ Number of ion units

S $\rightarrow$ Supersaturation

A_p $\rightarrow$ Activity product

K_{sp} $\rightarrow$ Solubility product (Equilibrium constant)

In the case of the present system, i.e. the formation of HAp by the reaction of $Ca(NO_3)_2.4H_2O$ and $NH_4H_2PO_4$,

n $\rightarrow$ Number of ion units in a calcium phosphate molecule

[n = 10+6+2 = 18, for $Ca_{10}(PO_4)_6(OH)_2$ molecule]

K_{sp} $\rightarrow$ Solubility product (Equilibrium constant)

[$(2.03 \pm 0.71) \times 10^{-59}$]

The supersaturation for HAp, $S = \dfrac{a^5(Ca^{2+})\, a^3(PO_4^{3-})\, a(OH^-)}{K_{sp}(HAp)}$

where *a* $\rightarrow$ Activity for each ion unit = Concentration $\times$ Activity coefficient (γ)

The change in Gibb's free energy for the solutions at different temperatures could be calculated using the Gibbs free energy equation if the size of the critical nucleus is measured.

2.2 Kinetics of Hydroxyapatite Formation:

Wet precipitation method based on the procedure is followed for the kinetics study. The reagent solutions of the selected system, calcium nitrate tetrahydrate [$Ca(NO_3)_2.4H_2O$] and ammonium dihydrogen orthophosphate [$NH_4H_2PO_4$] were prepared with definite concentrations so as to obtain the Ca/P ratio required to form HAp (1.67) and mixed at a definite temperature. The precipitation medium was made basic by addition of ammonia (NH_3) solution to the system. The precipitate formed was characterized using various techniques.

The main apparatus used for the synthesis are weighing balance, measuring flask, magnetic bead, magnetic stirrer with temperature probe, separating funnel, pH meter and centrifuge.

2.2.1 Wet precipitation method

Analytical grade Calcium nitrate tetrahydrate [$Ca(NO_3)_2.4H_2O$] (FINAR Chemicals, India), Ammonium dihydrogen orthophosphate [$NH_4H_2PO_4$] (RANKEM, India) and ammonia (RANKEM, India) for the work.

A typical wet synthesis was conducted as follows:

1. The reagents were weighed in required quantities so as to prepare a batch of a certain weight of HAp with a Ca/P molar ratio of 1.67.
2. The weighed reagents were dissolved in distilled water (H_2O) independently and the required quantity of ammonia (NH_3) solution was added to both the solutions separately.
3. The [$Ca(NO_3)_2.4H_2O$ + H_2O + NH_3] solution was heated to the desired temperature [temperature of synthesis-T_s] on a magnetic stirrer with temperature control and simultaneously stirred using a magnetic bead.
4. The $NH_4H_2PO_4$ + H_2O + NH_3 solution was added drop-wise to the calcium nitrate solution in 1 hour with continuous stirring at the desired temperature.
5. Stirring was continued for another hour maintaining the reaction temperature constant.

6. More NH_3 solution was added to the mixture after precipitation so as to obtain a basic pH of 9.
7. The mixture was kept for ageing, for 24 hours.
8. The mixture was washed in distilled water and centrifuged twice for 5 minutes each at 2500 rpm [HERAEUS Megafuge 2.0].
9. The precipitates obtained were stored at room temperature.
10. The above procedure was repeated for preparing HAp at a desired temperature of synthesis. Temperatures of 40°C, 50°C, 60°C, 70°C and 80°C were achieved by using heater. Precipitation at lower temperatures (20°C and 5°C) was done by keeping the solution in cold water/ice bath.

2.2.2. Processing of ceramic:

The processing involves the following procedures:

(i) Calcination : The precipitates were heated to 300°C in a high temperature programmable electrical furnace (OKAY raising hearth furnace model: 45R5Y) for removal of moisture and impurities.

(ii) Powdering and sieving: The calcined precipitates were powdered using a mortar and pestle. The powders were sieved into fine particles of size <125µm.

(iii) Compaction: 0.5g of the sieved powders of all the precipitates were pressed into discs in a stainless steel die of 13 mm diameter in a uniaxial press (SPEX-3630 X-PRESS) at a compaction pressure of 3 tons with 1minute holding time and 1minute releasing time.

(iv) Sintering: Sintering is the process of heating materials to elevated temperature, less than about three fourth of their melting temperature. Sintering is accompanied by shrinkage of the component, densification and formation of strong physical bonds between adjacent particles. The free energy of the system is decreased, which is the driving force for the sintering. During this process, a competition between densification and coarsening takes place. If densification is dominant then it will result in a dense body without many pores. But if coarsening is dominant, it will result in a highly porous body [27].

Sintering without the use of an externally applied pressure is referred to as conventional, free or pressure-less sintering [27]. In this method, a compacted disc of the sample is placed in a furnace where heat (radiation) from a hot source is transferred to it.

The samples, taken in crucibles, were loaded in the temperature programmable OKAY raising hearth furnace (model: 45R5Y) and heated to 1150°C temperature according to the program (fig.2.1).

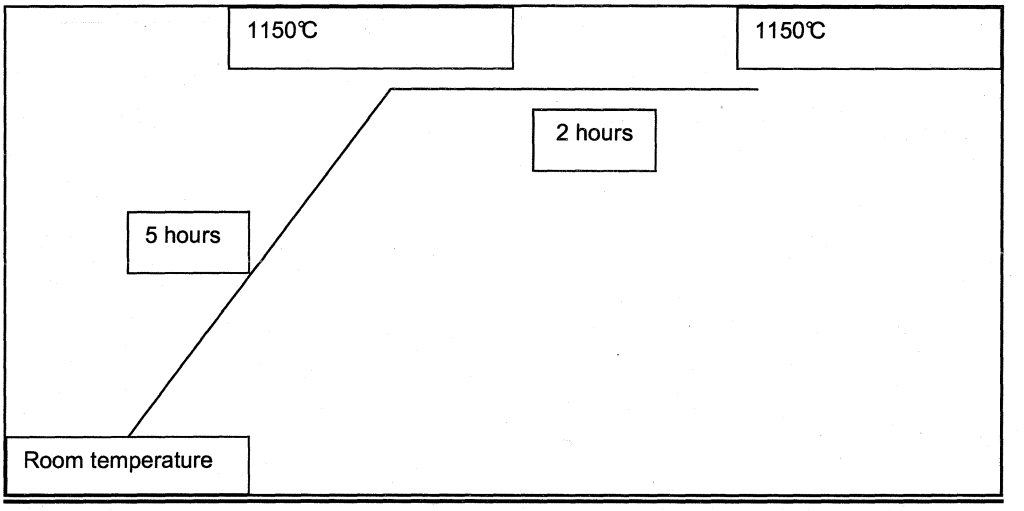

Fig 2.1 *Controller program for sintering*

(vi) *Polishing* : The specimens of compacts of all batches sintered at 1150℃ were polished with silicon carbide papers of grit sizes 240 and 600. They were finely polished further with a suspension of alumina (1.0 micron followed by 0.05 micron size) on a velvet cloth.

2.3 Characterization

The product of synthesis was subjected to vacuum drying in vacuum oven and ground into fine powder. Samples were taken from each batch and characterized by the following techniques.

2.3.1 X-ray powder diffraction

In the present study, the X-ray diffraction spectrum of each of the powdered samples were recorded using SEIMENS D-5005 X-ray diffractometer with vertical goniometer, with Cu Kα1 radiation (λ = 1.54056 A°), at 25 kV and 30mA, using a step size of 0.01°, scan rate of 1° p er minute with a scan range between 10° and 50° of 2 θ angle. The diffraction patterns of the samples were compared with the standards (JCPDS/ICDD files).

The particle size for each of the samples was calculated from the Full Width at Half Maximum (FWHM) of the peaks corresponding to the different crystal planes by employing the Debye Scherrer equation given by,

$$T = (K\lambda) / (\beta \cos\theta)$$

where T - Crystallite size, K - Constant (0.9), λ - X-ray wavelength (A°), β - Full Width at Half Maximum (radians) and θ- diffraction angle (°).

2.3.2 Fourier Transform Infrared Spectroscopy [FTIR]

Each of the powder samples was pressed into pellets after mixing with potassium bromide [1 wt % of KBr] reference with diameter 13 mm in a uni-axial press (SPEX-3630 X-PRESS) at a pressure of 7 tons with 1minute holding time and 1minute releasing time. Potassium bromide [KBr] reference pellets were also made. The FTIR spectrum of each sample pellet was recorded in the absorbance mode in Thermo-Nicolet 5700 FTIR spectrophotometer. Data were collected in the range 500 cm^{-1} to 4000 cm^{-1} at a resolution of 4 cm^{-1} (64 scans) after subtracting the background (64 scans in the reference pellet).

2.3.3 Dynamic light scattering [DLS] analysis

The precipitates as obtained after ageing of the product were dispersed in 1% w/w trisodium citrate solution and ultrasonicated. They were analyzed for particle size in DLS method in a particle size analyzer (Malvern nano ZS).

2.3.4 Transmission Electron Microscopy [TEM]

Specimens for TEM were prepared by dispersing the precipitates in ethanol with ultrasonic vibrator and spreading a small quantity on formvar-coated copper grids. TEM observations of the samples synthesized at temperatures 5℃, 20℃, 40℃, 60℃ and 80℃ were ma de in HITACHI TEM 7650, 120kV electron microscope.

2.3.5 Inductively Coupled Plasma [ICP] Technique

The ICP optical emission spectroscopy [ICP-OES] is a sensitive and accurate method for elemental detection and determination of the concentrations of the constituent ions of the molecular unit. The sample material in the dissolved form is excited to the plasma state [atoms/ions] by radio frequency discharge. The emission spectrum is detected by CCD detectors and recorded. The concentration of the ions in the system is obtained from the calibration plot of standards formulated in the same system.

Known quantities of vacuum-dried powders of the samples were dissolved in HNO_3 and subjected to ICP analysis [Perkin Elmer ICP-OES 5300 DV]. The Ca/P ratios are calculated from the calibration curves made with Ca and P standards.

2.3.6 Density measurement

According to the Archimedes principle,

Density = (Weight in air) ÷ (Weight loss in water)

The densities of all the compacted discs were measured using the Archimedes apparatus [attached to Sartorious Electronic Balance].

2.3.7 Microhardness measurement

Micro hardness testing involves forcing a pyramidal diamond indenter into the surface of the test material at loads ranging from 1 to 1000 gf. The hardness value is a measure of the resistance to penetration by an indenter under a localized force. In Vickers hardness testing, the value is determined by measuring the diagonal size of the resulting unrecovered indentation mark on a polished flat

sample surface, using a microscope. The test is done in accordance with standard established formulae [28].

The Vickers micro hardness of the samples were measured using Shimadzu Microhardness tester (HMV 2T), which uses a square-base diamond pyramid as the indenter. The angle between the opposite faces of the pyramid is 136°. Because of the shape of the indenter, the test is often called the diamond–pyramid hardness number (DPH) or Vickers Hardness Number (VHN) and is defined as the load applied divided by the surface area of the indentation. The Vickers hardness number is calculated using the following equation.

$$VHN = 2P \sin(\theta/2)/L^2 = 1.854\ P/L^2$$

where P is the applied load (kg), L is the average length of the diagonal (mm), and θ is the angle between the opposite faces of the diamond (136°).

2.3.8 Scanning Electron Microscopy [SEM]

According to Exner (1983), 'the microstructure is defined by the type, the structure and the number of phases, by the number, the geometric appearance (size, shape etc.) and the topological arrangement of the individual phase regions and their interfaces and by the type, structure and geometry of lattice defects'. The microstructure is determined by the synthesis and processing conditions and the composition of the material. The link between processing and properties of ceramic materials is represented by the microstructure of the material [29].

SEM is a technique based on the interaction of the specimen surface with the high-energy incident electron beam which reveals the surface microstructure of the specimen.

The polished discs of the samples were dipped in 0.01 M hydrochloric acid (HCl) solution for 1 minute time (chemical etching) for viewing the grain boundaries of the ceramic surface. Their microstructures were studied using 30 kV Environmental Scanning Electron Microscope (ESEM-Quanta 200, Germany).

2.3.9 Energy Dispersive X-ray (EDX) Analysis

The EDX system accepts and analyzes simultaneously, wavelengths from many elements. It is used to detect higher atomic number elements.

Interaction of the primary electron beam with the atoms of the specimen surface causes shell transitions, which result in the emission of x-rays. The emitted x-ray has an energy characteristic of the parent element. Detection and measurement of this energy enables elemental analysis. EDS can provide rapid qualitative, or with adequate standards, quantitative analysis of elemental composition with a sampling depth of 1-2 μm. EDS shows the elemental distribution on a sample surface.

The specimens were subjected to EDS studies coupled with ESEM [EDAX; OXFORD, X-ray microanalysis software].

Chapter 3

RESULTS AND DISCUSSION

3.1 Phase identification of the precipitate:

3.1.1 X-ray diffraction analysis

The XRD patterns of the samples synthesized at temperatures 5℃, 20℃, 40℃, 50℃, 60℃, 70℃ and 80℃ were recorded. The spectra were analyzed for phases by comparing with the JCPDS/ICDD files of various calcium phosphates. In all the samples, all the major peaks matched with that of hydroxyapatite (JCPDS 09-432). The XRD patterns obtained by slow scanning of samples corresponding to 5℃, 20℃, 50℃, 60℃ a nd 80℃ (along with standard diffraction lines for HAp) are given stacked in figure 3.1. In the whole range of synthesis temperature, the HAp phase was observed to be stable.

3.1.2 FTIR spectroscopy

The characteristic peaks corresponding to the constituent functional groups of HAp synthesized at various temperatures were identified from the FTIR absorbance spectra (Fig 3.2, as stacked series). The spectra are typical of hydroxyapatite, with characteristic peaks corresponding to hydroxyl (OH^-) and phosphate (PO_4^{3-}) groups in HAp molecule [$Ca_{10}(PO_4)_6(OH)_2$] (Table 3.1 shows the characteristic IR frequencies of HAp).

Wave number (cm^{-1})	***Peak characteristics***	
3670-3570 (sharp)	stretching vibration of OH^- ion	
3500-3100	Hydrated O-H	
1250 (weak shoulder)	HPO_4^{2-}	P-O-H in plane
760-720 (weak)		out-of-plane
1090, 1040-1014, 950-937, 601-597, 570-558, 470-420	PO_4^{3-}	
635-628 (medium sharp)	O-H bending deformation mode	

Table 3.1: *Characteristic IR frequencies of hydroxyapatite*

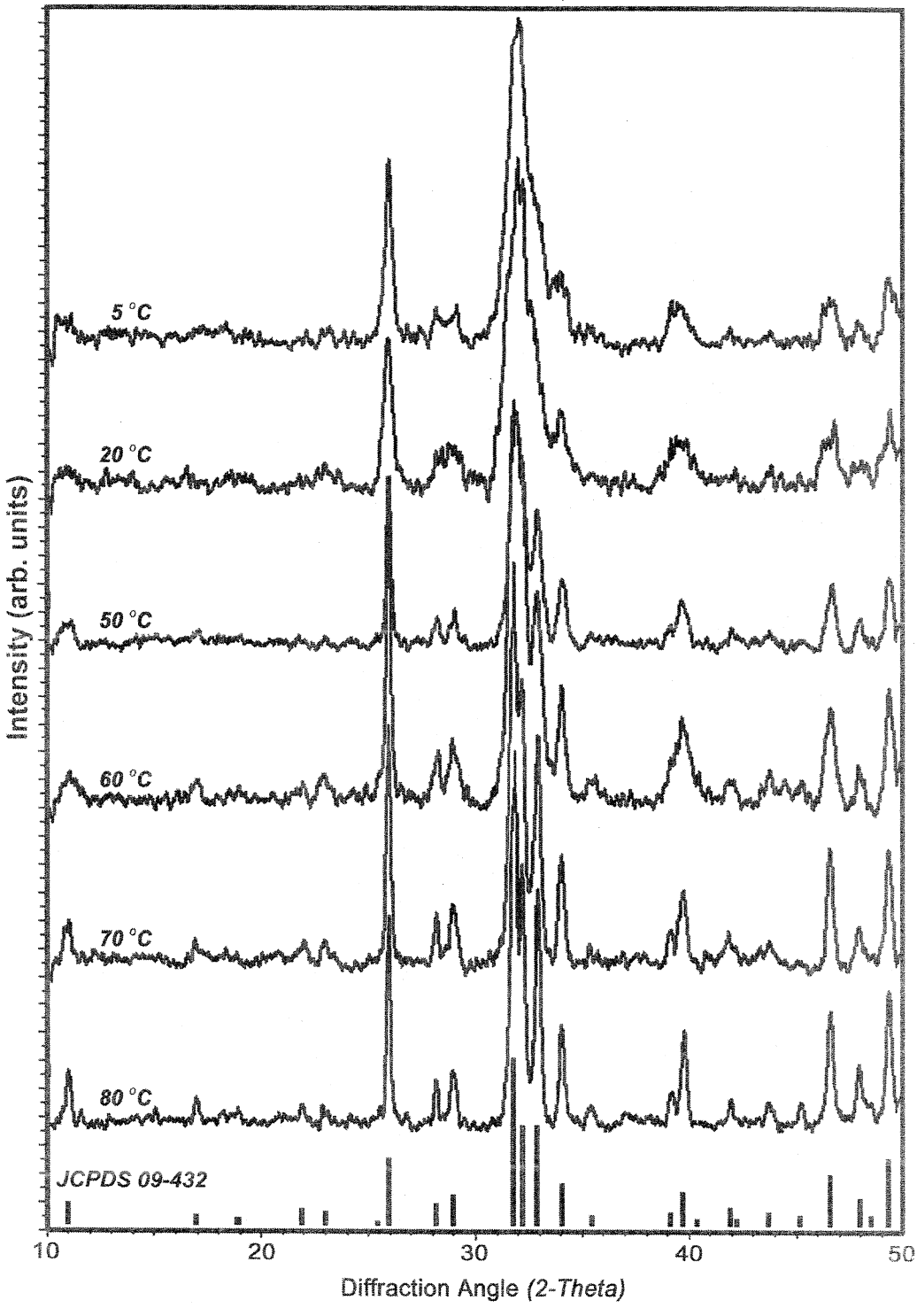

Figure 3.1 *XRD patterns of samples*

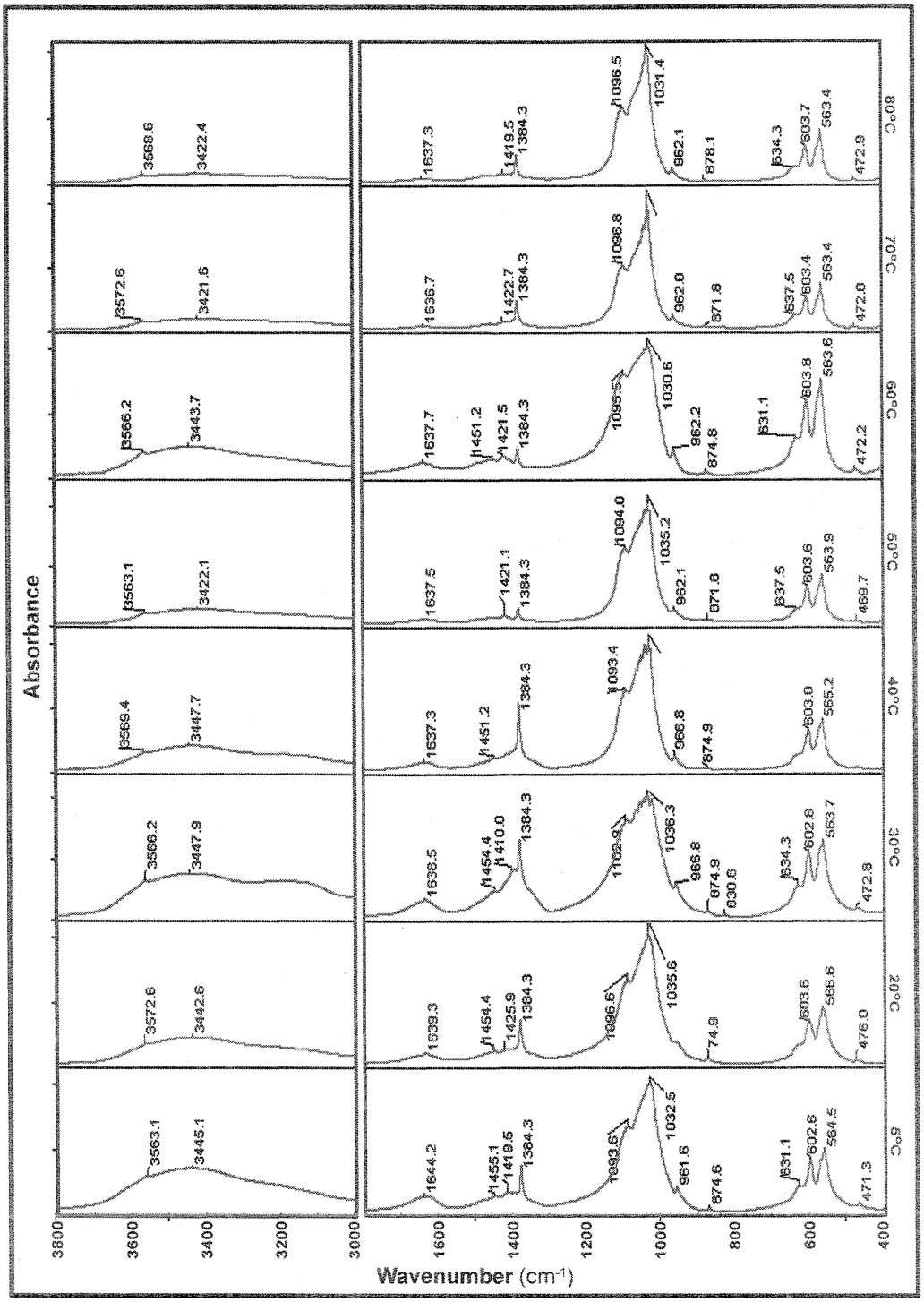

Fig. 3.2 *FTIR spectra of amorphous HAp prepared at different temperatures*

The peak near to 3570 cm^{-1} corresponds to the stretching vibration of the bound OH^- ion. The hydrated OH^- is represented by the broad peak in the region 3500 cm^{-1} – 3100 cm^{-1}. Carbonate groups, observed normally in natural HAp and occasionally in synthetic HAp, have peaks in the region 1650 to 1300 cm^{-1} (ν_3 bands) and around 873 cm^{-1} (ν_2 bands). In the present samples, these peaks are minimal, indicating the low carbonate content. All the theoretically predicted vibrational modes for phosphate ions (ν_1, ν_2, ν_3, and ν_4) are observed in the prepared HAp samples. The bands present in the region 1090 - 970 cm^{-1} confirm PO_4^{3-} in hydroxyapatite. The phosphate ν_1 and ν_4 bands are observed in the region 660 - 520 cm^{-1}. The presence of peaks at 631, 601, and 571 cm^{-1} indicate non-carbonated HAp. The FTIR data confirms the presence of the expected functional groups of hydroxyapatite in the precipitates of various temperatures.

3.1.3 Calcium / Phosphorous ratios

The Ca and P concentrations obtained from AES-ICP analysis and the calculated Ca/P ratios (by atomic weight) are listed in Table 3.2.

Synthesis Temperature (℃)	Ca concentration (µg/L)	P concentration (µg/L)	Ca/P ratio *
5	64.80	29.49	1.7029
20	68.03	33.39	1.5790
30	67.85	31.19	1.6859
40	69.33	34.18	1.5719
50	72.59	34.61	1.6255
60	67.64	30.78	1.7031
70	72.75	34.99	1.6003
80	75.53	34.65	1.6893
* (Ca concentration/Atomic Wt of Ca) ÷ (P concentration/Atomic Wt of P)			

Table3.2: *Ca/P ratios by ICP analysis of concentrations*

The Ca/P ratios vary from 1.57 to 1.7, which is comparable with the theoretical Ca/P ratio of hydroxyapatite, i.e. 1.67. The individual deviations are attributed to sample collection from the precipitating solution. The maturation time and leaching of Ca^{2+} ions back into washing solution may alter the Ca/P ratio in the collected sample.

3.1.4 The phase formation during precipitation

The analyses on the precipitates (phase analysis through XRD and functional group analysis through FTIR) and Ca/P ratio through AES-ICP formed at different temperatures indicate that phase-pure hydroxyapatite forms in the selected aqueous system [$Ca(NO_3)_2.4H_2O$ - $NH_4H_2PO_4$] at the experimental conditions. No other calcium phosphate phase appeared and the carbonate content was minimal. XRD and FTIR data indicate that the crystallinity and particle size of the precipitate decrease with lowering of the synthesis temperature.

3.2 Particle size analysis

3.2.1 Particle size through Debye-Scherrer method

On comparing the various XRD spectra given in fig. 3.1, it could be seen that the spectral peaks get broadened for the samples synthesized at lower temperatures (less than 30℃). The peaks become sharper for the samples synthesized at higher temperatures (above 50℃). This effect occurs due to the lowering of particle size. The broadening of diffraction lines is a useful means to find the particle sizes and the Debye-Scherrer equation, as explained in an earlier section, helps to calculate the same.

Normally, the first strong peak is selected for the Debye-Scherrer calculations. This is because, the theory holds better for such peaks. In the present case the (0 0 2) plane of HAp was selected. For cross-verification of the results, the (2 1 3) plane was also selected. Base-line correction of the peaks were done and a reasonable smoothening was given (through software) to read the angles conveniently. The peaking point was taken as the Bragg angle (θ) and the width of the peak was measured at the half height (at half of the counts of the peak). The crystallite size of the precipitates synthesized at various temperatures calculated from the (0 0 2) and (2 1 3) peaks are given in Table 3.3.

Synthesis Temperature (℃)	***Calculated crystallite size (nm)***	
	(0 0 2) plane	***(2 1 3) plane***
5	22.5	18.0
20	18.0	20.6
40	18.3	20.9
50	36.1	28.9
60	32.9	30.2
70	33.6	39.6
80	39.7	43.0

Table 3.3 *Variation in crystallite size with temperature of synthesis calculated from broadening of peaks*

3.2.2 Particle size through DLS

The DLS particle size results of samples prepared at various precipitation temperatures are presented in the figure set 3.3 **a** to **g**. The results of those at 5℃, 20℃ and 40℃ are presented as siz e distribution against % volume while those at 30℃, 50℃, 60℃ and 80℃ as size distribution against %intensity. DLS results of the samples show the average particle size distribution. Unimodal as well as bimodal distribution with lesser number of larger particles are observed. The results are tabulated in Table 3.4.

Synthesis temperature (℃)	***Particle size by DLS (nm)***
5	59.32
20	68.41
30	82.50
40	89.81
50	96.82
60	107.3
80	113.0

Table 3.4 *Particle size values obtained through DLS technique*

3.2.3 Particle sizes in TEM observations

The precipitates obtained at synthesis temperatures 5℃, 20℃, 40℃, 60℃, 80℃ were observed in TEM. The TEM images of each specimen at two different magnifications are presented in Fig.3.4 a to e. The particles were observed to be needle-shaped with progressing increase in length with temperature of synthesis. A particle size of ~40 nm is observed for the sample synthesized at 5℃, while a value of ~120 nm is obs erved for sample at 80℃. The particles are observed to have a strong tendency to aggregate. The average measured values for the samples are given in Table 3.5. As a general trend, as the synthesis temperature is increased, particle size also increases.

	Diam. (nm)	% Volume	Width (nm
Peak 1:	59.32	74.8	34.34
Peak 2:	4877	25.2	911.1
Peak 3:	0.000	0.0	0.000

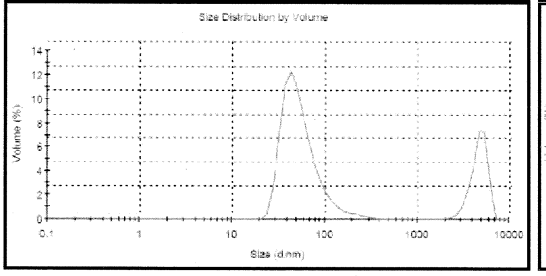

Fig. 3.3 (a) - at 5°C

	Diam. (nm)	% Volume	Width (nm)
Peak 1:	68.41	100.0	40.62
Peak 2:	0.000	0.0	0.000
Peak 3:	0.000	0.0	0.000

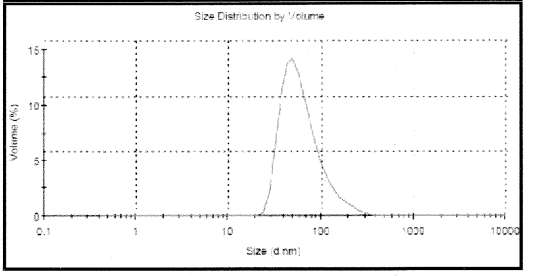

Fig. 3.3 (b) - at 20°C

	Diam. (nm)	% Intensity	Width (nm)
Peak 1:	82.50	94.9	32.38
Peak 2:	4850	5.1	700.6
Peak 3:	0.000	0.0	0.000

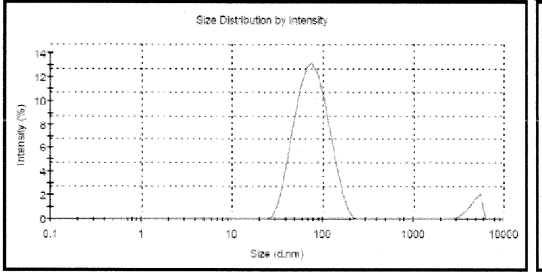

Fig. 3.3 (c) - at 30°C

	Diam. (nm)	% Volume	Width (nm)
Peak 1:	89.81	100.0	38.87
Peak 2:	0.000	0.0	0.000
Peak 3:	0.000	0.0	0.000

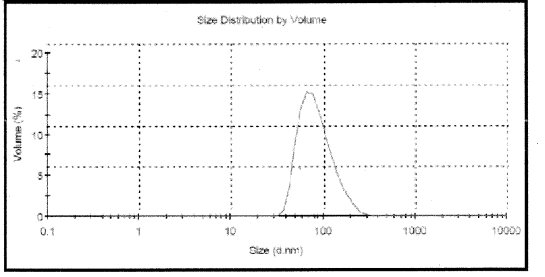

Fig. 3.3 (d) - at 40°C

	Diam. (nm)	% Intensity	Width (nm)
Peak 1:	96.82	96.9	51.73
Peak 2:	4582	3.1	837.7
Peak 3:	0.000	0.0	0.000

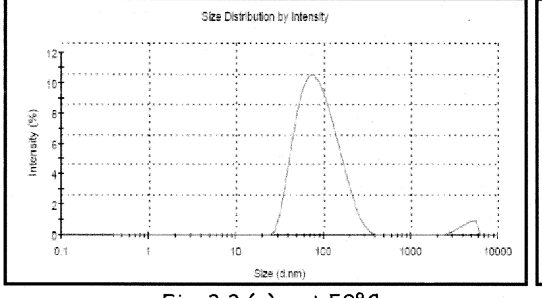

Fig. 3.3 (e) - at 50°C

	Diam. (nm)	% Intensity	Width (nm)
Peak 1:	107.3	100.0	52.37
Peak 2:	0.000	0.0	0.000
Peak 3:	0.000	0.0	0.000

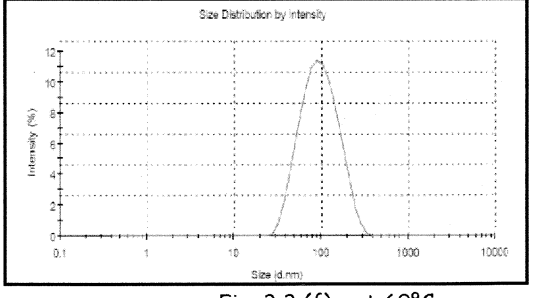

Fig. 3.3 (f) - at 60°C

	Diam. (nm)	% Intensity	Width (nm)
Peak 1:	113.0	100.0	59.86
Peak 2:	0.000	0.0	0.000
Peak 3:	0.000	0.0	0.000

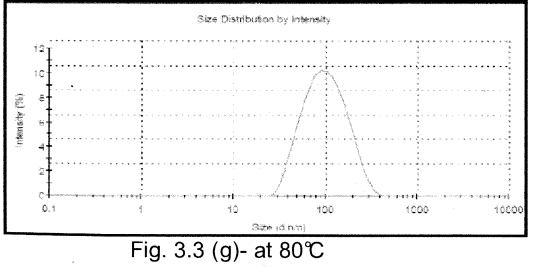

Fig. 3.3 (g)- at 80℃

Figure 3.3 **a** to **g** :

Average particle size by DLS

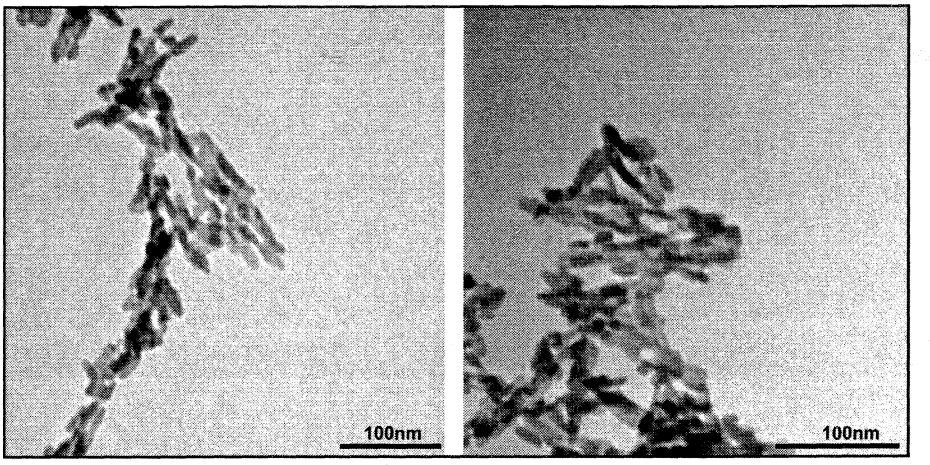

Fig 3.4 (a). *TEM images of HAp prepared at 5℃*

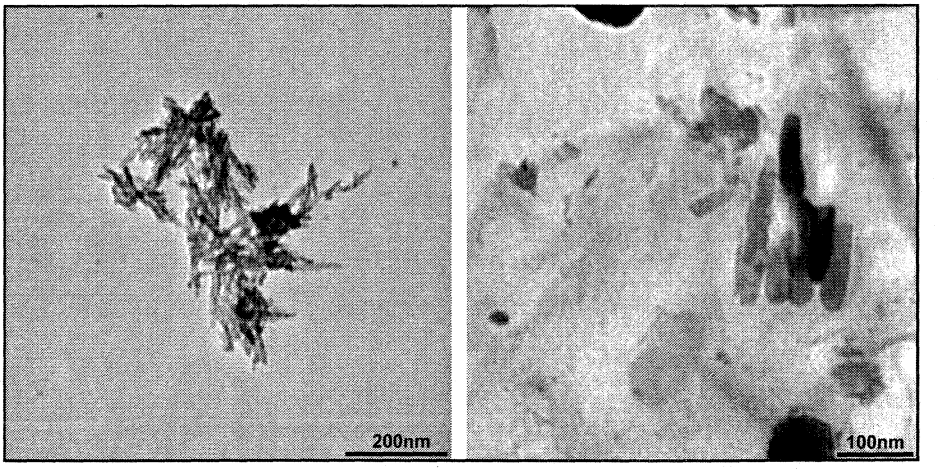

Fig 3.4 (b) *TEM images of HAp prepared at 20℃*

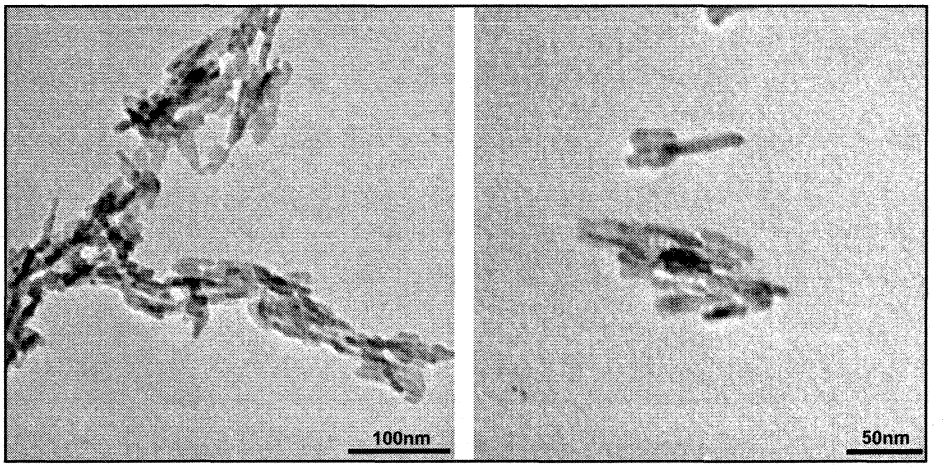

Fig 3.4 (c) *TEM micrographs of HAp prepared at 40℃*

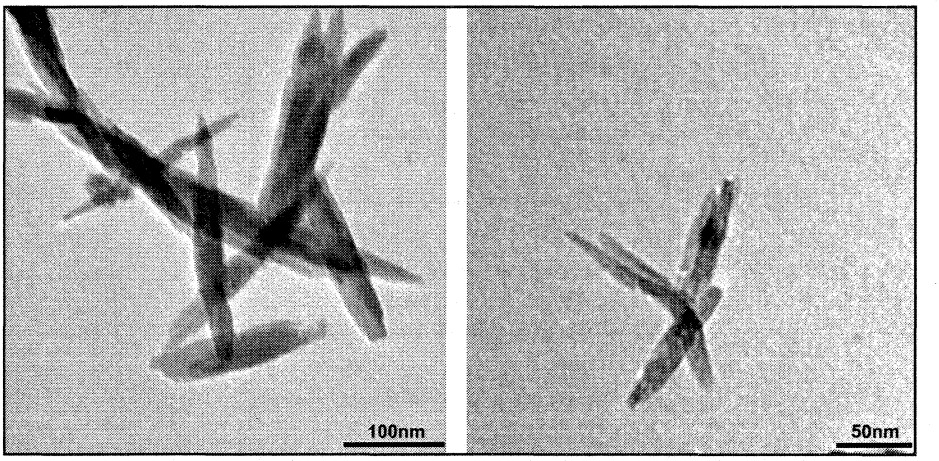

Fig.3.4 (d) *TEM micrographs of HAp prepared at 60℃*

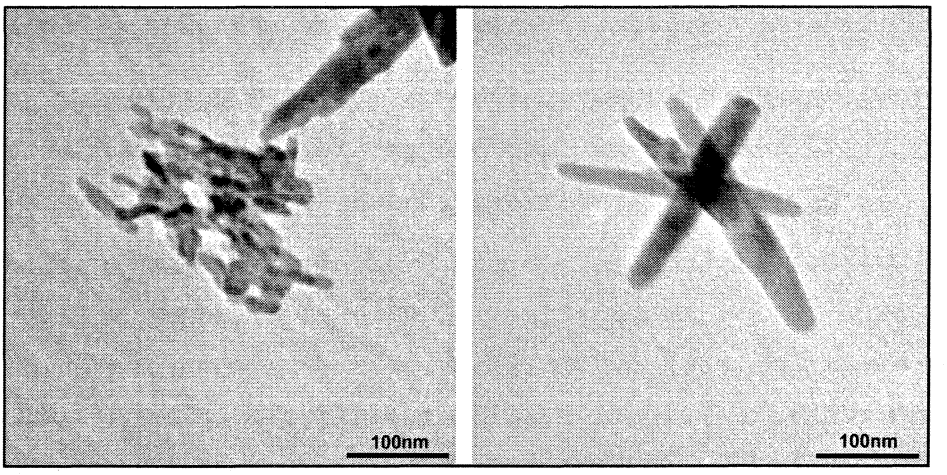

Fig.3.4 (e) *TEM micrographs of HAp prepared at 80℃*

Temperature (℃)	***Length (nm)***
5	40
20	50
40	60
60	100
80	120

Table 3.5 *Approximate lengths of particles from TEM images*

3.2.4 Results of the Particle size analyses

The particle sizes obtained in the precipitation at various temperatures were determined through 3 different techniques, which are conventionally used for the particle size measurements of nano materials.

The crystallite size calculations using the Debye-Scherrer equation, from the peaks corresponding to the (002) and (213) planes, are in the range of 18 nm - 40 nm. The values from the two different peaks seem to correlate well. The trend of reduction in particle size with decreasing synthesis temperature is evident from the peak broadening in the spectra (Fig 3.1). However, the reliability of the measurement depends on the averaging of the data points in the spectrum. Noises in the spectrum can influence the smoothening. Sufficient care is taken to minimize this effect. Despite this fact, the measured particle sizes through Debye-Scherrer method tend to be on the lower side because of possible broadening of the peaks due to machine parameters.

The limitation in the above method is evident from the results with DLS technique. The size variation trend is the same with the DLS technique (i.e., increase in particle size with increase in the synthesis temperature), but the sizes obtained are more than double compared to the XRD values and are in the range of 55nm to 115nm. In the DLS method, the values tend to be on the higher side, because HAp particles have the tendency to agglomerate. To avoid this, the precipitates were dispersed in appropriate media and vigorous ultrasonic stirring was given.

The ideal way to confirm the particle size is TEM analysis. This method, however, does not provide the size distribution in a sample (this is to be done manually from the images). The TEM images of the samples reveal the particle shape to be needle-like and their existence as chains/aggregates. The trend of increase in particle size with increase in the synthesis temperature was confirmed in TEM also.

3.4 Ceramic characteristics

3.4.1 Density measurement

The densities of the sintered HAp pellets prepared using the particles of different formation temperatures are presented in Table 3.6. This is graphically shown in Fig. 3.5. The values are within a narrow range of 2.89 – 3.1 g/cc and there is no observable trend of variation. This means the particle size difference does not affect the density significantly. Considering the theoretical density of HAp, (3.157 g/cm^3) the values obtained are the highest which is possible with the conventional method.

No.	*Particle formation Temperature (°C)*	*Density (g/cm^3)*
1	5	3.0464
2	20	2.9270
3	30	2.9142
4	40	2.8928
5	50	3.0771
6	60	3.0174
7	70	3.1086
8	80	3.0821

Table 3.6: *Density of sintered HAp measured by Archimedes method*

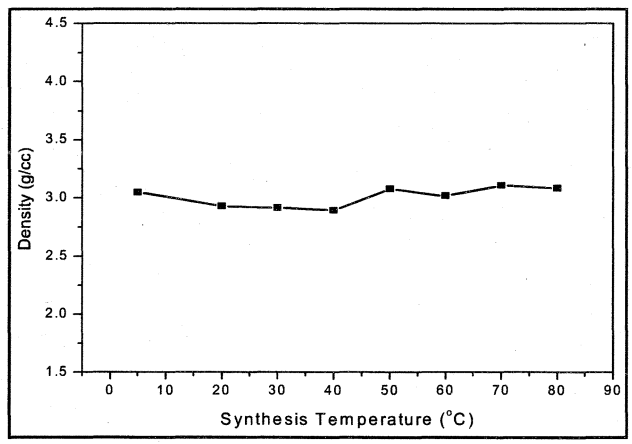

Fig.3.5. *Variation of density of sintered HAp*

3.4.2 Microstructure analysis by SEM

The ceramic samples made with HAp particles synthesized at various temperatures and sintered at 1150°C, were viewed under Environmental Scanning Electron Microscope after etching in mild acid (0.01M HCl). The electron micrographs were recorded with Back Scattered Electron Detector.

Gradual variation in grain sizes could be observed, with larger grains for lower synthesis temperature. Micrographs corresponding to 5℃ are given in figure 3.6 (a&b) and those for 80℃ sample are give n in figure 3.7 (a&b).

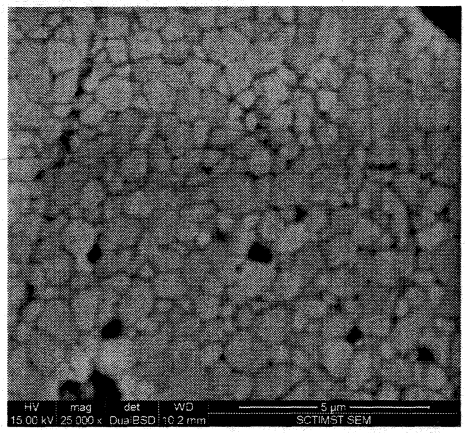

Fig 3.6 (a)

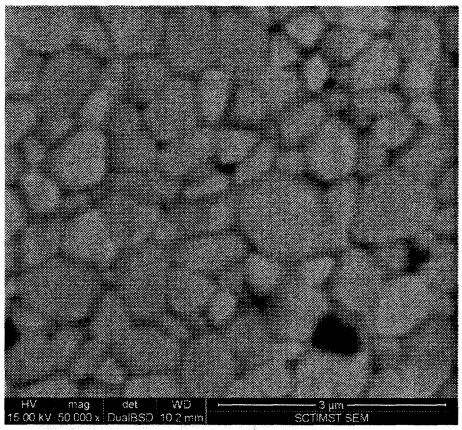

Fig 3.6 (b)

Fig.3.6 *SEM of sintered HAp prepared at a reaction temperature of 5°C*

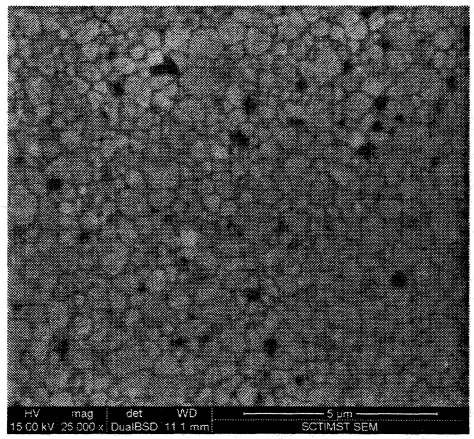

Fig 3.7 (a)

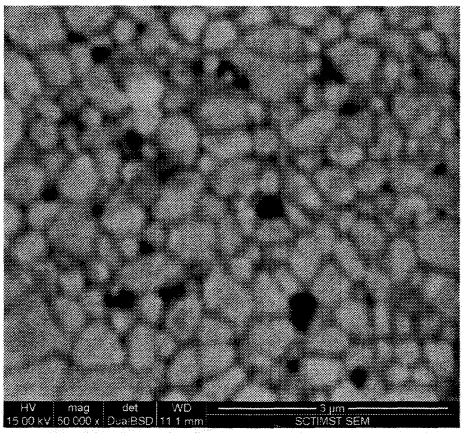

Fig 3.7 (b)

Fig.3.7 *SEM of sintered HAp prepared at a reaction temperature of 80°C*

Average grain size for samples synthesized at 80℃ was <1 μm, whereas a grain size of ~1.5 μm is observed for samples synthesized at 5℃. This variation in grain size is probably due to the effect of the (nano) particle size on the initial crystallite size formed during sintering. The sintering temperature may be higher than required for the lower-size particles (<50 nm) to form grains, than for higher-size particles (>100 nm).

The EDS spectra (X-ray emission energy versus intensity) of the same samples are as given in figure 3.8 (for 5℃ sample) and figure 3.9 (for 80℃ sample). The peaks corresponding to Ca, P and O could be seen. The Ca/P ratios could be verified.

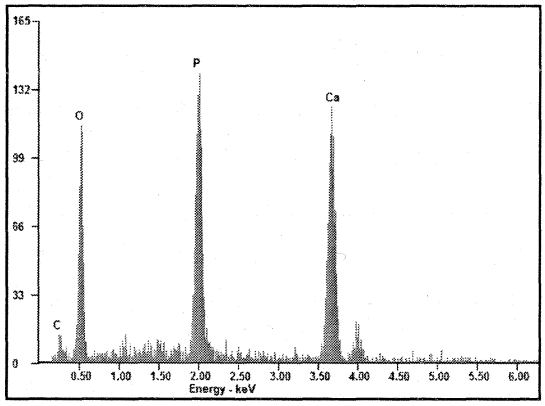

Fig 3.8 *EDS pattern sintered HAp prepared at 5°C temperature*

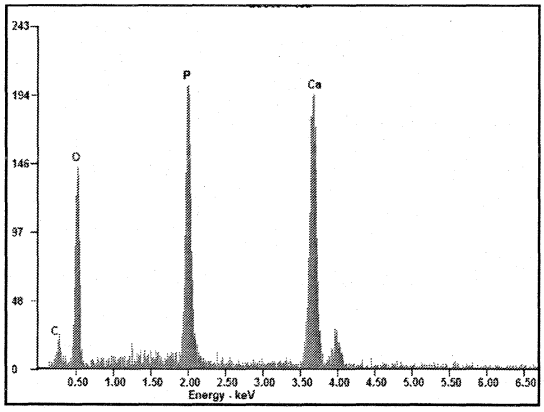

Fig 3.9 EDS *pattern of sintered HAp prepared at 80°C temperature*

3.4.3 Microhardness

The Vicker's microhardness values of the ceramic samples made with HAp particles synthesized at various temperatures were determined using the microindentation tester. The samples were prepared by pressing the powder as pellets and sintering at a temperature 1150°C, exactly similar to the samples for microstructure study. They were polished with SiC sheets of grit sizes 240 and 600 and subsequently with alumina paste (1.0 μ followed by 0.05 μ) smeared on polising cloth. The values (H_V) were measured at 6 different locations on each pellet with indentation load 100 gf, which are charted in Table 3.7. The trend of the mean values is represented graphically in figure 3.10.

It is observed that a Vicker's microhardness values of the HAp ceramics with lower particle sizes (lower synthesis temperature) is significantly reduced compared to those with higher particle sizes (higher synthesis temperature). The H_V for the 5℃ sample (191) is approximately three ti mes lesser than that for the 80℃ sample (581.67). The value obtained fo r the 80℃ sample is the highest H_V value reported for nano-hydroxyapatite ceramic [30].

Synthesis Temperature (℃)	***5***	***20***	***30***	***40***	***50***	***60***	***70***	***80***
HV1	205	233	211	336	431	482	539	565
HV2	162	236	231	360	391	477	531	597
HV3	187	203	285	336	495	473	546	571
HV4	198	238	332	321	491	477	523	609
HV5	190	207	343	347	486	453	546	571
HV6	204	340	310	342	464	481	526	577
Mean	**191.00**	**242.83**	**285.33**	**340.33**	**459.67**	**473.83**	**535.17**	**581.67**
SD	15.95	49.96	54.02	13.00	41.18	10.70	9.99	17.37

Table 3.7: *Microhardness values for ceramic pellets made with particles of various precipitation temperatures*

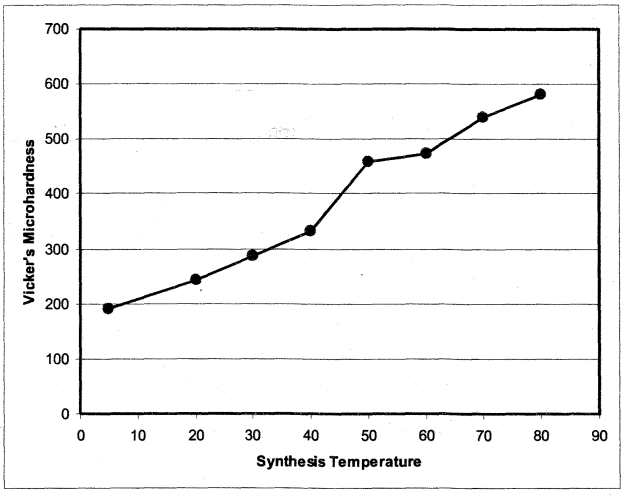

Fig 3.10 *Trend in the microhardness values for ceramic pellets made with particles of various precipitation temperatures*

3.4.4 Dependence of microhardness on microstructure

A drastic increase in microhardness is observed with the increase in particle size of the starting HAp material, when sintered at 1150℃. This increase, despite the close values of density, is notable. It could be explained with the microstructural features observed in the SEM analysis.

It could be seen in Fig 3.7 that the grains formed by the nanoparticles of 80℃ are small and more uniformly distributed. This microstructure has contributed to the high microhardness of the ceramic where as the microstructure formed by the nanoparticles of 5℃ shows a non-uniform distribution of larger and smaller grains (Fig 3.6). The minimum particle size obtained by the TEM analysis for the 5℃ synthesized sample is ~ 40 nm. Unequal distribution of larger grains formed on sintering may be attributed to agglomeration and growth enhancement of the smaller particles at such a high temperature. It is clear that the sintering temperature of 1150℃ is higher for the material of this particle size. Lesser particle-size samples may require only still lesser energy to form uniform and compact microstructure [25].

Chapter 4

SUMMARY AND CONCLUSION

This study is concerned with the formation of hydroxyapatite from aqueous solutions supersaturated with calcium and phosphate ions and the properties of ceramics made out of nano-sized HAp particles obtained through wet precipitation. Initially, a theoretical understanding was developed regarding the nucleation and growth of hydroxyapatite from such systems. The energy conditions imply that nanoparticles form in such a system and the particle size will be directly proportional to the formation temperature.

An aqueous system containing calcium nitrate tetrahydrate [$Ca(NO_3)_2.4H_2O$] and ammonium dihydrogen orthophosphate [$NH_4H_2PO_4$] was selected for the study. The reactions were conducted at controlled conditions and precipitates of different reaction temperatures, from 5℃ to 80℃, were collected. The phase stability of the product formed was confirmed through techniques like XRD and FTIR. It was found that phase - pure HAp was formed at all temperature conditions. Both XRD and FTIR spectra indicated the presence of HAp nanoparticles in the precipitates, particularly at all the synthesis temperatures in the range 5℃ to 80℃.

Particle size measurements of the precipitates formed at different temperatures, from 5℃ to 80℃, were done using thr ee different techniques. In the first method, Debye-Scherrer equation was applied to the prominent diffraction peaks in the XRD pattern to deduce the crystallite size from the peak width. The peaks corresponding to the (002) and (213) planes gave particle sizes in the range 18 nm - 40 nm for 5℃ to 80℃ pr ecipitates. Although there are only slight differences between the consecutive values, the enlargement of crystallites with increase in synthesis temperature was evident. DLS technique also was used for particle size determination, which clearly established that the particle size increased with increase in the synthesis temperature. The particle sizes were within the range of 55nm - 115nm (for samples of 5℃ to 80℃). The TEM images revealed the particle shape to be needle-like and their existence

as chains/aggregates. The particle sizes measured by TEM imaging were 40nm - 120 nm (for samples of 5℃ to 80℃), which c orrelated with the DLS results.

In the latter part of the experiment, pellets of the HAp material obtained at different temperatures from 5℃ to 80℃, were ma de through conventional ceramic techniques. All the samples were compacted equally and sintered at 1150°C. Densities of these ceramics obtained for various particle sizes were within a narrow range (2.8 - 3.1 g/cc), which is in a higher range obtainable for conventional HAp ceramics.

Microstructure analysis of these nano-HAp ceramics by ESEM revealed larger grain size and non-uniform grain distribution for the 5℃ samples while smaller grain size and more uniform distribution were observed for the 80℃ samples.

The Vicker's microhardness measurements showed a drastic increase as the particle size (or synthesis temperature) increases. The H_V values varied from 191 for the 5℃ sample to 581.67 for the 80℃ sample. This effect could be explained with the microstructural features.

The outcomes of this study give the following conclusions:

In aqueous precipitation, hydroxyapatite starts forming as nanoparticles. It is possible to synthesize a desired set of nano-sized HAp from aqueous solution by optimizing the parameters. Highly dense and hard ceramic could be produced with nano-sized HAp by carefully adjusting the sintering temperature. Nano-based HAp ceramics, as described in this work, are highly useful in certain orthopaedic applications like vertebro-laminoplasty.

To have better products in this line, optimization of precipitation conditions and careful sintering are required. More studies on the nucleation and crystal growth of HAp from aqueous solutions and also on the ceramic processing parameters are necessary to achieve this goal.

Reference

1. Takahashi. Calcium apatite prepared from calcium hydroxide and orthophosphoric acid. J. Mater. Sci.: Mater. in Med, January 1991; 2: 51-55.

2. Lopez-Macipe A, Rodriguez-Clement R, Hidalgo- Lopez A, Arita I, Garcia-Garduno M V, Rivera E and Castano VM. Wet chemical synthesis of hydroxyapatite particles from nonstoichiometric solutions. J. Mater. Synth. Proc, January 1998; 6: 21-26.

3. Zhang S, Gonslaves K E. Preparation and characterization of thermally stable nanohydroxyapatite. J. Mater. Sci.: Mater. in Med. 1997; 8: 25-28.

4. Chai C S and Ben-Nissan B. Bioactive nanocrystalline sol-gel hydroxyapatite coatings. J. Mater. Sci.: Mater. In Med, 1999; 10: 465-469.

5. Xu Y, Wang D, Yang L and Tang H. Hydrothermal conversion of coral into hydroxyapatite. Mater. Character, 2001; 47: 83-87.

6. Yadav KL.and Brown PW. Formation of hydroxyapatite in water, Hank's solution and serum at physiological temperature. J. Biomed. Mater. Res. A, 2003; 65A: 158-163.

7. LeGeros, R Z. Properties of Osteoconductive Biomaterials: Calcium Phosphates. Clinical Orthopaedics & Related Research. 2002; 395 : 81-98

8. Lazi S. Microcrystalline hydroxyapatite formation from alkaline solutions. J. Crys. Growth, 1995; 147:147-154.

9. Suchanek W and Yoshimura M. Processing and properties of hydroxyapatite-based biomaterials for use as hard tissue replacement implants. J. Mater. Res, 1998; 13: 94-117.

10. Narasaraju, S B and Phebe, D. E. Some physicochemical aspects of hydroxyapatite J. Mater. Sci. 1996; 31: 1-27.

11. Aoki H. Medical Applications of Hydroxyapatite. Ishiyaku EuroAmerica, Inc.: Tokyo, 1994.

12. Heise U, Osborn JF and Duwe F. Hydroxyapatite ceramic as a bone substitute. International Orthopaedics.1990; 14, (3): 329-338, DOI: 10.1007/BF00178768

13. Asaoka, N.; Best, S.; Knowles, J. C.; Bonfield, W. Bioceramics, 1995; 8: 331-337.

14. Kumar, R.; Prakash, K. H.; Cheang, P.; Khor, K. A. Langmuir, 2004;20: 5196-5200.

15. Liu C, Huang Y, Shen W and Cui J. Kinetics of hydroxyapatite precipitation at pH 10 to 11. Biomaterials 2001; 22 : 301-306

16. Mullins JW. Crystallization. 2nd Edition, Cleveland: CRC Press; 1972: 219.

Reference

1. Takahashi. Calcium apatite prepared from calcium hydroxide and orthophosphoric acid. J. Mater. Sci.: Mater. in Med, January 1991; 2: 51-55.

2. Lopez-Macipe A, Rodriguez-Clement R, Hidalgo- Lopez A, Arita I, Garcia-Garduno M V, Rivera E and Castano VM. Wet chemical synthesis of hydroxyapatite particles from nonstoichiometric solutions. J. Mater. Synth. Proc, January 1998; 6: 21-26.

3. Zhang S, Gonslaves K E. Preparation and characterization of thermally stable nanohydroxyapatite. J. Mater. Sci.: Mater. in Med. 1997; 8: 25-28.

4. Chai C S and Ben-Nissan B. Bioactive nanocrystalline sol-gel hydroxyapatite coatings. J. Mater. Sci.: Mater. In Med, 1999; 10: 465-469.

5. Xu Y, Wang D, Yang L and Tang H. Hydrothermal conversion of coral into hydroxyapatite. Mater. Character, 2001; 47: 83-87.

6. Yadav KL.and Brown PW. Formation of hydroxyapatite in water, Hank's solution and serum at physiological temperature. J. Biomed. Mater. Res. A, 2003; 65A: 158-163.

7. LeGeros, R Z. Properties of Osteoconductive Biomaterials: Calcium Phosphates. Clinical Orthopaedics & Related Research. 2002; 395 : 81-98

8. Lazi S. Microcrystalline hydroxyapatite formation from alkaline solutions. J. Crys. Growth, 1995; 147:147-154.

9. Suchanek W and Yoshimura M. Processing and properties of hydroxyapatite-based biomaterials for use as hard tissue replacement implants. J. Mater. Res, 1998; 13: 94-117.

10. Narasaraju, S B and Phebe, D. E. Some physicochemical aspects of hydroxyapatite J. Mater. Sci. 1996; 31: 1-27.

11. Aoki H. Medical Applications of Hydroxyapatite. Ishiyaku EuroAmerica, Inc.: Tokyo, 1994.

12. Heise U, Osborn JF and Duwe F. Hydroxyapatite ceramic as a bone substitute. International Orthopaedics.1990; 14, (3): 329-338, DOI: 10.1007/BF00178768

13. Asaoka, N.; Best, S.; Knowles, J. C.; Bonfield, W. Bioceramics, 1995; 8: 331-337.

14. Kumar, R.; Prakash, K. H.; Cheang, P.; Khor, K. A. Langmuir, 2004;20: 5196-5200.

15. Liu C, Huang Y, Shen W and Cui J. Kinetics of hydroxyapatite precipitation at pH 10 to 11. Biomaterials 2001; 22 : 301-306

16. Mullins JW. Crystallization. 2nd Edition, Cleveland: CRC Press; 1972: 219.

17. Onuma K and Ito A. Cluster growth model for hydroxyapatite. Chem Mater 1998;10:3346–3351.

18. Zhu P, Masuda Y, Koumoto K. The effect of surface charge on hydroxyapatite nucleation. Biomaterials, 2004; 25: 3915–3921.

19. Prakash KH, Ooi CP, Kumar R., Khor KA. Cheang P. Effect of Super Saturation Level on the size and morphology of Hydroxyapatite precipitate. IEEE, 2006: 345-349.

20. Chow LC. and Sun L and Hockey B. Properties of Nanostructured Hydroxyapatite Prepared by a Spray Drying Technique. J. Res. Natl. Inst. Stand. Technol, 2004;109: 543-551.

21. Vasconcelos IF, Pimenta MA, Sombra ASB. Optical properties of Bi12SiO20 (BSO) and Bi12TiO20 (BTO) obtained by mechanical alloying. J Mat Sci , 2001; 36(3): 587-592.

22. Stupp SI, Ciegler GW. Organoapatites: materials for artificial bone. I. Synthesis and microstructure. J Biomed Mater Res, 1992; 26(2): 169-183.

23. Webster TJ, Ergun C, Doremus RH, Siegel RW, Bizios R. Enhanced osteoclast-like cell functions on nanophase ceramics. Biomaterials, 2001; 22(11): 1327-1333.

24. Murugan R, Rao KP, Kumar TSS. Heatdeproteinated xenogeneic bone from slaughterhouse waste: Physico-chemical properties. Bull Mater Sci, 2003; 26(5): 523-528.

25. Suresh Babu S, Vijayan S, Varma HK. Transparent hydroxyapatite ceramics through gelcasting and low temperature sintering. J.Am.Ceram.Soc., 2002 ; 85 [2] : 493-495.

26. Ralph H. Obenauf, Richard Bostwick, Mena Mc Cann, Joan D. Mc Cormack. Robert Merriman. David Selem. Hand book of sample preparation and handling.

27. Rahman MN. Ceramic processing. CRC Press 2007.

28. Metals Hand Book -9th edition. Volume-8. Mechanical testing.

29. Materials Science and Technology- A comprehensive treatment- Edited by E.W.Cahn, P.Haasen, E.J.Kramer- Processing of ceramics-Part I.

30. Fomin AS., Barinov SM, Levlev VM, Smirnov VV, Mikhailov BP, Kutsev SV,. Belonogov EK, Drozdova NA, Nanocrystalline hydroxyapatite ceramics, Inorganic Materials 2009; 45 [10] : 1193-1196.